



LAWRENCE
LIVERMORE
NATIONAL
LABORATORY

Flash X-Ray Resolved Trajectory of Discrete Particles from Embedded Explosive Detonation

M. J. Murphy, D. E. Stevens

June 2, 2014

15th International Detonation Symposium
San Francisco, CA, United States
July 14, 2014 through July 18, 2014

Disclaimer

This document was prepared as an account of work sponsored by an agency of the United States government. Neither the United States government nor Lawrence Livermore National Security, LLC, nor any of their employees makes any warranty, expressed or implied, or assumes any legal liability or responsibility for the accuracy, completeness, or usefulness of any information, apparatus, product, or process disclosed, or represents that its use would not infringe privately owned rights. Reference herein to any specific commercial product, process, or service by trade name, trademark, manufacturer, or otherwise does not necessarily constitute or imply its endorsement, recommendation, or favoring by the United States government or Lawrence Livermore National Security, LLC. The views and opinions of authors expressed herein do not necessarily state or reflect those of the United States government or Lawrence Livermore National Security, LLC, and shall not be used for advertising or product endorsement purposes.

Flash X-Ray Resolved Trajectory of Discrete Particles from Embedded Explosive Detonation

David E. Stevens and Michael J. Murphy
Lawrence Livermore National Laboratory
8000 East Avenue, L-098, Livermore, California, 94551

Abstract. Flash radiography experiments and modeling are used to diagnose the trajectory of discrete particles from their initial detonic acceleration to a fluid regime more typical of a blast wave in air. High temporal and spatial resolution multi-frame radiography is used to visualize high density discrete particles moving through lower density explosive detonation products. These experiments focus on isolated particles as this provides the simplest possible fluid-particle interaction for a discrete particle accelerated by a detonation wave and its subsequent interaction with the immediate detonation products. Corresponding computational analysis was conducted with discrete particles in coupled Cheetah - ALE3D simulations. The experiments and discrete particle simulations have allowed for the derivation and evaluation of particle interaction models that assume semi-analytic solutions for particle-interactions. Extension of these models to include thermal and chemical kinetic effects is recommended.

Introduction

The analysis of particle trajectories in rapidly accelerating flow fields is complicated by many factors. Before complicated assessments of fluid-particle interactions can be made it is important and useful to understand the behavior of isolated particles under non steady state conditions. Flash radiography is a very attractive experimental technique for this regime as it combines both high temporal and spatial resolution with the ability to image particles through fluid regimes where the background medium varies in density from 1-2 grams/cc to near vacuum or where the background medium is opaque. These experiments track the isolated particles (via radiography) as they are accelerated by a detonation wave and their subsequent interaction with the immediate detonation products and air. The analysis of the experimental results is combined with simulations of discrete particles in coupled Cheetah-ALE3D^{1,2} simulations. The combination of high fidelity material and hydrodynamic modeling will be shown to greatly facilitate the

derivation and evaluation of particle interaction models that assume semi-analytic solutions for particle-interactions.

Experimental Method

The experiments consist of tracking the evolution of arrays of particles embedded in an explosive charge. The evolution of this charge after detonation is tracked by the experimental configuration shown in Figure 1, which consists of a rectangular array of four x-ray heads and a very large film cassette behind the charge to capture the dispersion of the particles. The area of the film cassette has been partitioned to progressively widen the field of view as the embedded particles disperse. The two initial radiographs make up the left third of the X-ray cassette (Images 1 and 2 in Figure 1) whereas the final two radiographs take up the bulk of the film on the right (Images 3 and 4) This division of the film allows for simple rectangular collimation.

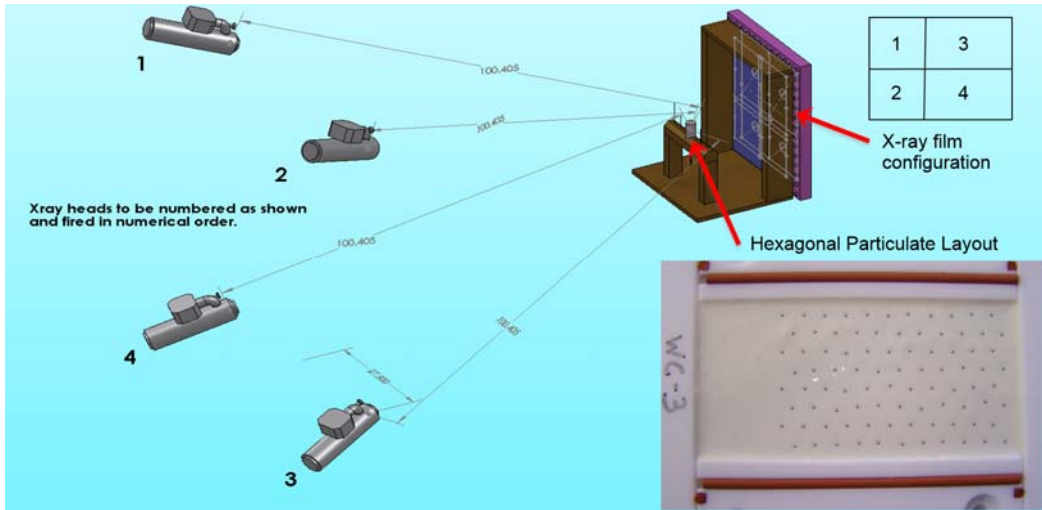


Fig. 1. Overview of the isolated particle experiment and hexagonal embedded particle layout

The explosive charges consisted of particles embedded in the mid-plane of a 2-inch diameter by 4-inch high cylinder of LX-20 HE. Different arrays of particles were used to create a wide range of particle-fluid interactions. The rectangular array of particles used in experiment WC2 is shown below in Figure 2. LX-20 was chosen as an explosive, due to its success in a prior experimental campaign by Murphy and Ames³ to diagnose the role of atmospheric pressure and liner systems in determining particulate arrival times and shock wave pressures. Embedding the particulate in the mid-plane of the charge produced a simplified

experimental geometry where the particulate only disperses in the radial and axial directions of the mid-plane.

The list of particle arrays used in our experiments is given in Table 1. This unique configuration of 8 tests allowed us to investigate simultaneously the role of particle size, density and initial position in the charge. The densities of the particulate were varied by using both tungsten (W) and tungsten-carbide (WC) particles. The rectangular (R) arrays of particles were stratified from top to bottom in particle size. The tests W2 and WC2 had rows of



Fig. 2. Rectangular particle layout for WC2.

Table 1. Test list and particulate loading

Test	Comp	Particle Layout	Bottom Dia (mm)	Top Dia (mm)
W1	W	R	0.65	1.55
W2	W	R	1.55	0.65
W3	W	H	0.65	0.65
W4	W	H	1.10	1.10
WC1	WC	R	0.60	1.20
WC2	WC	R	1.20	0.60
WC3	WC	H	0.60	0.60
WC4	WC	H	1.00	1.00

particles that transitioned from small diameters on the bottom of the charge closest to the detonator to large particles on the top of the charge (figure 2). The reverse stratification was used in tests W1 and WC1. This combination of tests helps differentiate the role of axial position in determining the eventual dispersion of a particle, such as the paired set of charges W1 and W2. The remainder of the charges used a hexagonal (H) type of layout (lower right image shown in figure 1) which was chosen to provide a high spatial density of information for fixed size and density of particulate. The hexagonal distribution has the advantage that it is very easy to differentiate particles from one radiograph to the next and that when one takes advantage of radial symmetry the density of data points is effectively doubled.

Another advantage of the hexahedral layout is that it has the potential to generate 88 distinct particle trajectories versus only 44 trajectories for a charge that was radially symmetric. Both particle layouts were separated from the bottom detonator by one inch of explosive to allow for a relatively planar detonation wave to develop before it impacted the lowest level of embedded particles. Each particle layout was repeated with two different particle compositions, which systematically incorporates the experimental dimension of particulate mass to particle size and location to the study. The need to resolve the particles by radiography forced the use of the high Z materials tungsten and tungsten carbide. The range of particles sizes used was chosen in the interest of being able to discretely resolve the particle positions. This limits the effectiveness of this study for smaller particle sizes. However as this was primarily a study of isolated particulate interacting with detonation waves and the subsequent dispersion, one can make self-similarity arguments about them being useful for smaller particle sizes.

Test Configuration and Results

The eight experimental charges provide a wide variety of particle densities, radii and positions within the charge. All of the tungsten-carbide (WC) experiments had X-ray images where each particle's Lagrangian trajectory was easily discernable for long periods of time. In the WC3 experiment, that is highlighted below, we were able to track all the particles up to 90 microseconds. However, all of the tungsten particulate shattered soon after impact. This is shown in Figure 3, which compares W3 against the analogous tungsten carbide experiment WC3 slightly later in time.

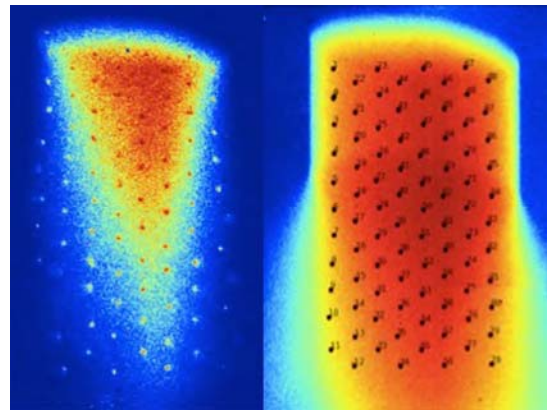


Fig. 3 W3 radiograph compared to WC3 .

All of the tungsten carbide (left frame) is discernable whereas the tungsten particulate (right frame) is easily discernable above the detonation front; it is discernable only as fuzzy entities after the detonation front. Fortunately, the tungsten charges W3 and W4 are self-similar along the axial direction with respect to the detonation front. Hence, the particles at the top of the charge are equivalent to the particles at the bottom of the charge earlier in time. This indicates that figure 3 contains by itself a fair amount of temporal information about particle breakup. Simulations described below were performed to help diagnose these phenomena.

Drag Model

Simulation studies were considered for both fractured and intact particulate which represents the two post detonation configurations observed. Particles can shatter upon impact with the detonation wave or they can survive to be tracked in a Lagrangian trajectory. For the particles that survive, it is possible to organize the analysis around equation 1 that describes the particle momentum.

$$\frac{\partial u_p}{\partial t} = \frac{1}{\tau_v} (u_g - u_p) + \frac{\alpha_g \rho_g}{\alpha_p \rho_p} \left((1 + R) \frac{\partial u_g}{\partial t} - R \frac{\partial u_p}{\partial t} \right) \quad (1)$$

This equation treats particle acceleration or deceleration as a combination of standard drag effect that takes into account a particle being decelerated by a constant velocity background fluid and acceleration on the particle caused by its being embedded in an accelerating fluid and, hence, being accelerated by that fluids stress state. The drag effect is formulated using an empirical relaxation time constant, τ , that functions as an inverse drag coefficient. The quantities in the budget are the particle velocity, u_p , gas velocity, u_g , particle volume fraction, α_p , and density, ρ_p , and the fluid volume fraction, α_g and density, ρ_g . The factor, R , comes from the work done by the fluid on the particle and, for incompressible flow, has a value of 0.5.

Lagrange Trajectories

The data from the tungsten carbide shots enabled us to construct Lagrangian trajectories for all of these experiments. Figure 4 shows the Lagrangian trajectories for all the particles in experiment WC3. Radial symmetry was used to flatten the hexagonal array into four axial rows of 22 particles each. The diagnosed experimental trajectory for each row is depicted using a different color. The outline

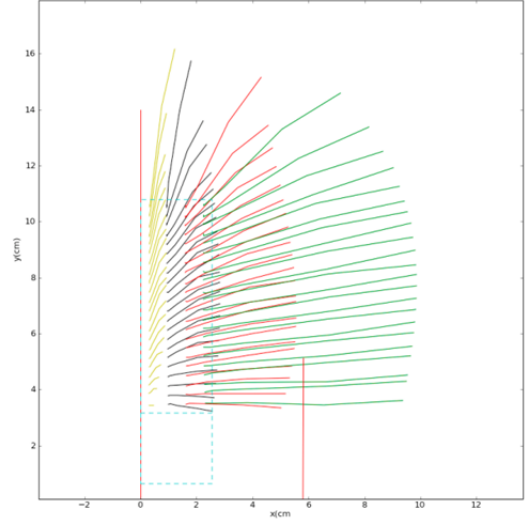


Fig. 4 Reconstructed particle trajectories

of the charge is in light blue and the bottom inch containing no particles is also shown. One feature that is easily discernable is the fact that particles on the edge of the charge are accelerated to a much larger extent than those in the center of the charge. This arises from the fact that the outer particles see a much larger pressure gradient and much larger fluid velocities than those at the center of the charge. The goal of our analysis below is to use these Lagrangian trajectories in combination with modeling from ALE3D to diagnose parameters of interest in validating the ALE3D model.

Computational Analysis

The first computational analysis used embedded discrete particles in an ALE3D simulation that consists solely of an LX-20 cylinder surrounded by air. The detonation front was calculated as a simple “programmed burn” based on a lighting time that is just the distance from the bottom center of the charge to a desired point in the charge. The detonation velocity of LX-20 is a well-known quantity, and the ability of ALE3D to simulate a simple HE charge detonation has been well validated.

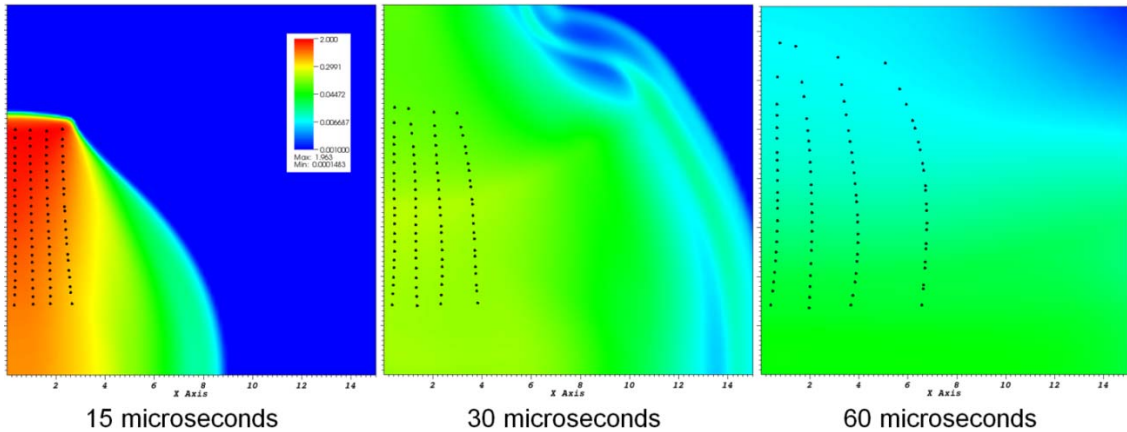


Fig. 5. Reconstructed particle trajectories overlaying fluid densities at 15, 30, and 45 microseconds.

A unique new feature in ALE3D is the ability to couple inline to CHEETAH with conduction and viscosity models in addition to equilibrium chemistry and chemical kinetics. This gives ALE3D the rather unique ability to recreate the fluid properties that surround each of the particles as it moves along its trajectory. The experimentally diagnosed position of each particle in experiment WC3 is shown superimposed over the background fluid density in Figure 5 for three periods of time.

The rapid drop in working fluid velocity is shown in each frame. Note that the particles remain embedded in the HE product gases in all of the frames shown. This approach makes it easy to determine many of the quantities in our particle momentum budget and several other quantities that are usually of interest such as Reynolds Numbers. The time histories shown in Figure 6 for each of the particles indicate a rapid transition from a high Reynolds number region to a lower one and that the velocity difference between the fluid and the particles rapidly decreases. Unfortunately, this technique has difficulties directly diagnosing the actual terms in our momentum equation. This difficulty arises from two sources of error. The first source arises from the fact that taking second differences of

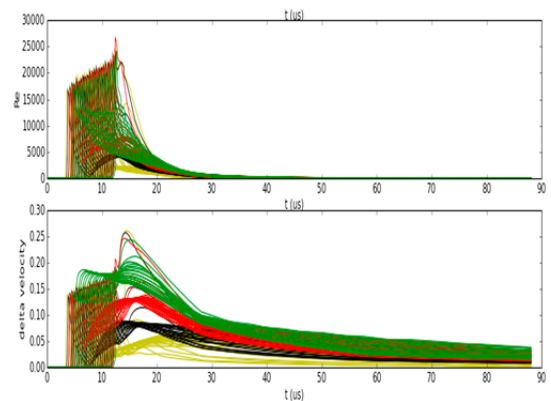


Fig. 6. Reconstructed Reynolds numbers (top) and fluid-particle velocity differences

experimental data amplifies experimental errors. The second source arises from the fact that we are only able to create trajectories out of only four data points. Eliminating this second source of error would require several more X-ray images for each experiment. Figure 7 shows the diagnosed drag coefficient where the only simulation derived quantities are the fluid properties associated with each point along the trajectory. The very large values of the drag coefficient at early times arise from contamination of the momentum budget from inaccurately accounting for the detonation phase. The large values at the end of the experimental time interval are due to the first source of error

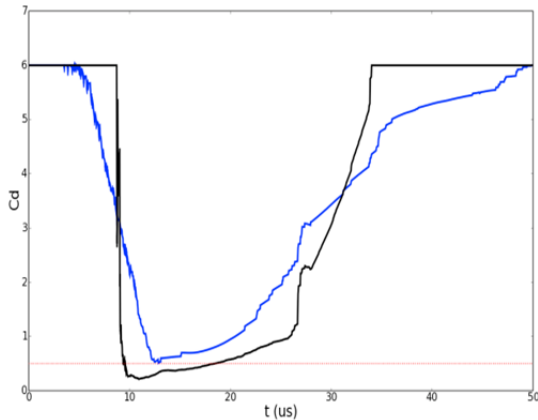


Fig. 7. Drag coefficient from WC3 test

affecting our ability to accurately detect the slow acceleration of the particle. There is also some error due to extrapolating particle acceleration to the end of the time interval. It should be noted that the more physically meaningful values of the drag coefficient occur where the temporal density of the data is greatest and the acceleration error from the detonation is no longer present.

An alternative analysis of the momentum budget can be obtained using analytic particle trajectories. The value of each term in the budget is found optimizing the drag coefficient and R parameter to yield final particle positions that match the experimental data. This approach suffers from overly relying on numerical models and the optimal result could be arrived at by a misleading combination of compensating errors. The analytic particles that represent the optimal fit of our budget to our experimental data at 60 microseconds are shown in Figure 8. Fortunately, the optimal drag coefficient from our simple gradient method was 0.47. However, the optimal R value was very close to zero, which is probably not accurate. This anomalous R value prompted us to compute a two-dimensional study of the values that minimize the quadratic error between the experimental and analytic particles. The results of which are shown in Figure 9. Here, we see that the drag term and the

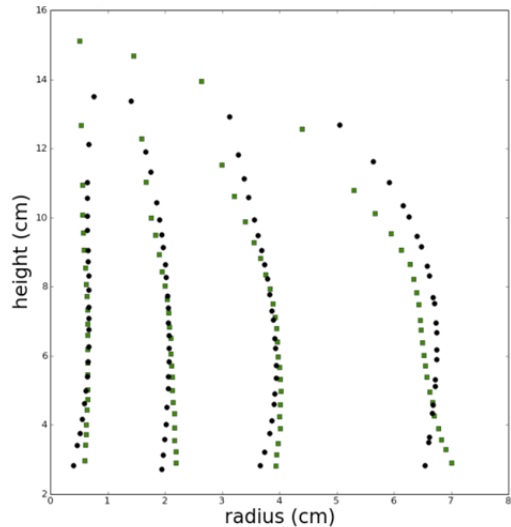


Fig. 8. Comparison of simulation (green) and experiment (black).

fluid acceleration terms are correlated with each other. This is seen by the long flat valley of minimum error. The error minimum easily encompasses the 0.5 value of R in the incompressible limit. Fortunately, the minimum errors are encompassed by drag coefficients between 0.4 and 0.6. This indicates that the drag coefficient of 0.5 is indeed a reasonable value for use in more complex simulations.

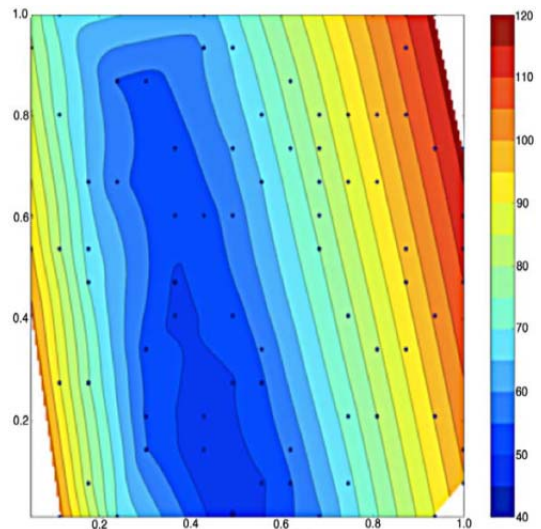


Fig. 9. 2-D parameter study of error

Summary

The ability of the simulated discrete particles to replicate the observed particle dynamics has several important ramifications. Probably, the most important of these ramifications is that we can now derive or evaluate advanced particle interaction models that assume semi-analytic solutions for particle-interactions. This is a preliminary requirement for extending our models to eventually include thermal and chemical kinetic effects.

The use of inline Cheetah coupled to ALE3D provides potentially the most accurate treatment of viscosities and conductivities that go into sophisticated particle evolution models. A drag coefficient of 0.5 is a reasonable value to use for applied simulations.

References

- 1 L. E. Fried, K. R. Glaesemann, W. M. Howard, P.C. Souers and P. A. Vitello, "Cheetah Code," Lawrence Livermore National Laboratory, UCRL-CODE-155944 (2004).
2. A. L. Nichols, "ALE3D, An Arbitrary Lagrange/Eulerian 2D and 3D Code System, Volume 1, General Information," Lawrence Livermore National Laboratory, LLNL-SM-650174 (2014).
3. Ames, R. G, and Murphy, M. J., "Diagnostic Techniques for Multiphase Blast Fields," 24th International Symposium on Ballistics (2008).

Acknowledgements

The authors would like to acknowledge the support from the following individuals at the Lawrence Livermore National Laboratory: Stan Ault, S300 bunker team, and Jason Gwo.

This work was funded by the Joint DoD/DOE Munitions Technology Development Program, and matching funds were provided by DOE. This work was performed under the auspices of the U.S. Department of Energy by Lawrence Livermore National Laboratory under Contract DE-AC52-07NA27344.